DOI: 10.14218/JCTH.2025.00237

Original Article



Inflammation and Mitochondrial Dysfunction in Cirrhotic Cardiomyopathy: Therapeutic Implications



Yijie Ding^{1#}, Chengfeng Huang^{1#}, Guannan Yang², En Liu¹, Zhongxin Wang³, Yong Su^{1,4*} and Chaoliang Ge^{1,4*}

¹Department of Pharmacy, The First Affiliated Hospital of Anhui Medical University, School of Pharmacy, Anhui Medical University, Hefei, Anhui, China; ²Department of General Surgery, Graduate school of Wannan Medical College, Wuhu, Anhui, China; ³Department of Clinical Laboratory, The First Affiliated Hospital of Anhui Medical University, Hefei, Anhui, China; ⁴The Grade 3 Pharmaceutical Chemistry Laboratory of State Administration of Traditional Chinese Medicine, Hefei, Anhui, China

Received: May 21, 2025 | Revised: September 05, 2025 | Accepted: September 18, 2025 | Published online: October 20, 2025

Abstract

Background and Aims: Cirrhotic cardiomyopathy (CCM) is a significant complication of cirrhosis, but its progression and underlying mechanisms remain incompletely understood. This study aimed to investigate dynamic changes in cardiac function, pathology, inflammation, and mitochondrial damage in a mouse model of CCM, and to compare echocardiographic characteristics in patients with cirrhosis. Methods: Bile duct ligation was performed in male C57BL/6J mice to induce cirrhosis. Longitudinal analyses were conducted over eight weeks. Cardiac function was assessed using serum biomarkers, echocardiography, and electrocardiography. Pathology was examined with hematoxylin and eosin, Masson's trichrome, Sirius Red, and wheat germ agglutinin staining. Western blotting and immunohistochemistry were used to detect markers of inflammation, fibrosis, apoptosis, and mitochondrial function. Cardiac and liver function markers were also evaluated in patients with cirrhosis. Results: Mice subjected to bile duct ligation developed progressive cardiac dysfunction, including reduced cardiac output and diastolic dysfunction (enddiastolic interventricular septal thickness, left ventricular internal diameters, stroke volume, and left ventricular end-diastolic volume decreased, whereas ejection fraction and fractional shortening increased), as well as cardiac atrophy. Myocardial apoptosis, inflammation (elevated tumor necrosis factor, interleukin-6, and p65), and fibrosis worsened over time. Mitochondrial injury was characterized by reduced carnitine palmitoyltransferase 1A and peroxisome proliferator-activated receptor alpha, with increased hexokinase 2, pyruvate kinase M2, and lactate dehydrogenase A. In patients with cirrhosis, impaired cardiac function and elevated brain natriuretic peptide levels correlated with total bilirubin. *Conclusions:* The progression of CCM is closely associated with cirrhosis severity and appears to

be driven by myocardial atrophy, apoptosis, inflammation, fibrosis, and mitochondrial dysfunction.

Citation of this article: Ding Y, Huang C, Yang G, Liu E, Wang Z, Su Y, *et al.* Inflammation and Mitochondrial Dysfunction in Cirrhotic Cardiomyopathy: Therapeutic Implications. J Clin Transl Hepatol 2025. doi: 10.14218/JCTH.2025. 00237.

Introduction

Cirrhotic cardiomyopathy (CCM) is a cardiac disorder that occurs in patients with cirrhosis, independent of other heart diseases. It is characterized by an impaired contractile response to stress, diastolic dysfunction, and a prolonged QT interval.¹ Reported prevalence ranges from 26% to 81%,² but the mechanisms underlying cirrhosis-induced cardiac injury remain unclear, and no specific preventive treatments for CCM have yet been developed.

The 2005 World Congress of Gastroenterology established diagnostic criteria for CCM, which were later revised in 2020 by the Cirrhotic Cardiomyopathy Consortium.³ Since then, numerous studies have examined its pathophysiology and clinical course before transplantation, although research using animal models remains limited. Existing animal studies have produced inconsistent findings regarding the timing and mechanisms of injury, with conflicting results on cardiac hypertrophy, atrophy, and impaired contractile function at rest.^{4–7}

Uhlig *et al.* conducted a detailed investigation of temporal dynamics and cardiac fragility in a rat model, but the absence of gallbladders in rats may limit the applicability of their findings to CCM.⁸ In contrast, Matyas *et al.* evaluated heart function in mice with bile duct ligation (BDL)-induced cirrhosis and showed that mice reproduce the pathophysiological features of CCM.⁷ Nevertheless, the two-week study period was insufficient to capture the dynamic progression of the disease.

This study assessed cardiac function in mice with BDL-induced cirrhosis at weeks 2, 4, and 8, while also examining dynamic changes in inflammatory and mitochondrial markers. In addition, echocardiographic data were collected from patients with CCM to analyze the correlation between cirrhosis severity and cardiac dysfunction.

Keywords: Cirrhotic cardiomyopathy; Liver cirrhosis; Myocardial dysfunction; Fibrosis; Apoptosis; Mitochondria. *Contributed equally to this work.

^{*}Correspondence to: Yong Su and Chaoliang Ge, Department of Pharmacy, The First Affiliated Hospital of Anhui Medical University, Hefei, Anhui 230032, China. ORCID: https://orcid.org/0000-0002-0082-1146 (CG). Tel/Fax: +86-551-65908530, E-mail: suyong@ahmu.edu.cn (SY) and gechaoliang@126.com (CG).

Methods

Animal model

All animal care and experimental procedures were approved by the Ethics Committee of Anhui Medical University (LLSC20210241) and conducted in accordance with the Declaration of Helsinki (2024). Seventy male C57BL/6J mice (seven weeks old, 20-25 g) were purchased from Jiangsu Jicui Pharmaceutical Biotechnology Co., Ltd. The mice were housed under controlled conditions with an ambient temperature of 24 ± 1°C, a 12-h light/dark cycle, and a relative humidity of 55% ± 5%. Before the study, they were acclimated to the laboratory for one week and then randomly divided into five groups using a randomized block design: Control, Sham, two weeks, four weeks, and eight weeks. There were 14 mice in each group. Since the survival rate of BDL surgery is only about 50%, 14 mice were included in each group (a total of 70) to ensure a final sample size of n = 6 per group. BDL surgery was performed in all groups except the Sham group, which underwent the same procedure without ligation. BDL was conducted as previously described.9 At the endpoint, mice were fasted for 8 h, anesthetized with isoflurane (R510-22-10; RWD, China), and euthanized by cervical dislocation following orbital blood sampling (~0.2 mL). Death was confirmed by an audible click from cervical vertebral dislocation, followed by the absence of heartbeat and spontaneous respiration. The heart and liver were then rapidly excised. Potential confounding by cirrhosis severity and comorbidities was considered, and efforts were made to collect standardized echocardiographic and biochemical data.

Patient cases of liver cirrhosis

Data were collected from 65 patients with liver cirrhosis treated at the First Affiliated Hospital of Anhui Medical University between 2021 and 2025. The inclusion criteria required a diagnosis of liver cirrhosis with no history of cardiovascular disease. The control group consisted of 39 healthy individuals who underwent routine physical examinations at the same hospital. Informed consent was obtained from all patients and healthy controls. This study was approved by the Biomedical Ethics Committee of Anhui Medical University (Ethics Number: PJ2024-05-76), and all procedures complied with the ethical principles of the Declaration of Helsinki and the International Ethical Guidelines for Biomedical Research.

Echocardiography

Mice were anesthetized with isoflurane (R510-22-10; RWD, China), and two-dimensional M-mode echocardiography was performed at two, four, and eight weeks using a VINNO 6LAB ultrasound system (VINNO, China). The E/A ratio was assessed by pulsed Doppler echocardiography, and the E/e' ratio was measured by tissue Doppler echocardiography.

Electrocardiography

Mice were anesthetized with isoflurane (R510-22-10; RWD, China) and placed in the supine position on the table, secured with tape. Subcutaneous needle electrodes from a commercial electrocardiography system (BL-420F; Chengdu Tailian Technology Co., Ltd., China) were then attached to record the electrocardiogram.

Treadmill exercise performance test

Mice were first acclimated to the treadmill for $5\,$ min at an initial speed of $2\,$ m/min. The speed was then increased by

2 m/min every 2 min up to a maximum of 16 m/min. The test was terminated when a mouse remained on the active electric grid at the rear of the treadmill at least 18 times for more than $10 \, \mathrm{s}$ each.

Blood pressure measurement

Systolic blood pressure and diastolic blood pressure were measured at the tail using a Softron BP-2010 animal sphygmomanometer. Before the formal test, all mice were trained to adapt to the measurement procedure. Measurements were obtained while the mice were calm in a warm (37°C), dark environment. Blood pressure was measured at least three times, and the average value was recorded.

Histopathology

Fixed tissues were sectioned at a thickness of 5 μm for histological analysis. Sections were stained with hematoxylin and eosin (B006 & B005; ebiogo, China), Masson's trichrome (B022; ebiogo, China), wheat germ agglutinin (L4895; Sigma-Aldrich, USA), and 0.1% Sirius Red (BP-DL030; Sbjbio, China) following the manufacturers' protocols. Stained sections were examined and imaged using a 3D HISTECH Panoramic MIDI system, and whole-slide scans were analyzed with CaseViewer software.

Terminal deoxynucleotidyl transferase dUTP nick end labeling (TUNEL) staining

TUNEL staining was performed as previously described. 10 After deparaffinization, cardiac tissue sections were incubated with 20 µg/mL DNase-free protease, followed by TUNEL detection solution. The reaction was terminated with labeled reaction stop solution, after which streptavidin–horseradish peroxidase working solution was applied. After washing, 3,3'-diaminobenzidine tetrahydrochloride color development solution was added, and the sections were counterstained with hematoxylin. Finally, the sections were differentiated with 1% hydrochloric acid–ethanol solution. Stained sections were examined and imaged using a 3D HISTECH Panoramic MIDI system, and whole-slide scans were analyzed with CaseViewer software.

Immunohistochemistry

Immunohistochemistry was performed as described previously. 11 Fixed tissues were sectioned at a thickness of 5 µm for immunohistochemical analysis. The expression of interleukin (IL)-1 β , IL-6, p65, and tumor necrosis factor (TNF) was detected using microwave-assisted antigen retrieval. Sections were incubated overnight at 4°C with primary antibodies: mouse anti-IL-1 β (1:50), rabbit anti-IL-6 (1:50), mouse anti-p65 (1:50), and rabbit anti-TNF (1:50). After incubation with the appropriate secondary antibodies, staining was visualized using 3,3'-diaminobenzidine tetrahydrochloride, and the slides were counterstained with hematoxylin. Stained sections were examined and imaged using a 3D HISTECH Panoramic MIDI system, and whole-slide scans were analyzed with CaseViewer software.

Western blotting

Western blotting was performed as previously described. ¹² Total protein was extracted from treated heart tissue using radioimmunoprecipitation assay lysis buffer (P0013B; Beyotime, China) supplemented with protease inhibitors (P1005; Beyotime, China) and phosphatase inhibitors (ST506-2; Beyotime, China). Protein concentrations were determined using the BCA Protein Assay Kit (P0010; Beyotime, China). Equal amounts of protein were separated by sodium dode-

cyl sulfate-polyacrylamide gel electrophoresis (8%-12%) and transferred onto polyvinylidene fluoride membranes (P2120; Millipore, USA). Membranes were blocked with 5% skim milk for 1 h at room temperature and then incubated overnight at 4°C with the following primary antibodies: Bcell lymphoma 2 (Bcl-2; 1:1,000, 60178-1-Ig; Proteintech, China), Bcl-2-associated X protein (Bax; 1:1,000, 60267-1-Ig; Proteintech, China), caspase-3 (1:1,000, 19677-1-AP; Proteintech, China), lactate dehydrogenase A (LDHA; 1:1,000, 19987-1-AP; Proteintech, China), pyruvate kinase M2 (PKM2; 1:1,000, 60268-1-Ig; Proteintech, China), carnitine palmitoyltransferase 1A (CPT1A; 1:1,000, 15184-1-AP; Proteintech, China), phosphorylated p65 (1:1,000, PAB53260; Bio-Swamp, China), p65 (1:1,000, MAB51128; Bio-Swamp, China), and β -actin (1:10,000, 81115-1-RR; Proteintech, China). After washing, membranes were incubated for 1 h at room temperature with either anti-rabbit (1:10,000, ZB-2301; Origene, China) or anti-mouse (1:10,000, SA00001-1; Proteintech, China) secondary antibodies, followed by additional washing. Protein bands were visualized using an enhanced chemiluminescence reagent (BL161A; Biosharp, China), and densitometric analysis was performed with ImageJ software.

Reverse transcription quantitative polymerase chain reaction (RT-qPCR)

Total RNA was extracted from snap-frozen heart tissue using TRIzol reagent (Invitrogen, Grand Island, NY, USA). RT-qPCR was performed with SYBR® Green and mouse-specific primer sets. Relative gene expression was calculated using the $2^{-\Delta\Delta Ct}$ method, with normalization to glyceraldehyde-3-phosphate dehydrogenase. ¹³ The primer sequences used in this study are listed in Supplementary Table 1.

Electron microscopy

Animals were euthanized with an overdose of isoflurane (RWD, China). A 1 mm³ piece of cardiac tissue was excised with a surgical blade and immediately fixed in 2.5% glutaraldehyde for 24 h. The fixed tissue was embedded in pure epoxy resin and sectioned at a thickness of 70 nm for histological analysis. Sections were stained with Grade B stain (22400; Electron Microscopy Sciences, USA) and examined using a transmission electron microscope (JEM1400; JEOL, Japan).

Statistical analysis

Data are expressed as mean \pm standard error. Group differences in normally distributed data were analyzed using oneway analysis of variance followed by Tukey's post hoc test, performed with GraphPad Prism version 9.5 (GraphPad Software, San Diego, CA, USA). Non-normally distributed data were analyzed using the Kruskal–Wallis test in SPSS version 17 (IBM Corp., Armonk, NY, USA). Categorical variables were compared using the chi-squared test. Each experiment was repeated three times, and statistical significance was defined as p < 0.05.

Results

BDL-induced liver injury and cirrhosis in mice

Pathological examination of the liver was performed across the five groups of mice. After BDL, mice developed severe cholestasis by two weeks, which progressively worsened and led to reduced liver weight (Fig. 1A). Serum analysis showed significant increases in alkaline phosphatase, aspartate aminotransferase, alanine aminotransferase, and

total bilirubin at two weeks, indicating liver dysfunction. Aspartate aminotransferase levels rose at two weeks, then declined at four to eight weeks but remained higher than those in the control group (Fig. 1B). Histological assessment revealed extensive structural changes. Hematoxylin and eosin staining showed distorted liver architecture in mice after BDL, with marked ductal proliferation, enlarged hepatocyte nuclei, hepatocyte swelling, pseudolobule formation, and inflammatory cell infiltration. By two weeks, partial confluent necrosis appeared in the central region around the lesion, and the necrotic areas expanded progressively (Fig. 1C). Masson's trichrome staining demonstrated intense collagen deposition around the central hepatic vein, with fibrosis evident in the hepatic bile ducts. Morphological analysis revealed dark-stained masses with pronounced radial adhesion of collagen fibers in hepatocytes, and the degree of fibrosis increased steadily over time (Fig. 1D). Together, these pathological findings confirmed that mice subjected to BDL developed severe liver injury, progressing to cirrhosis by four weeks.

BDL-induced cardiac dysfunction in mice

Echocardiography was performed to evaluate cardiac function. Mice subjected to BDL showed impaired cardiac performance, with significant reductions in end-diastolic interventricular septal thickness, end-diastolic left ventricular internal diameter, end-systolic left ventricular internal diameter, stroke volume (SV), left ventricular end-diastolic volume, cardiac output, and heart rate. Notably, the decreases in end-systolic left ventricular internal diameter, SV, left ventricular end-diastolic volume, and cardiac output at two weeks were more pronounced than those observed at four weeks. These changes were accompanied by bradycardia and thickening of the left ventricular posterior wall at the end of systole. Although left ventricular ejection fraction (EF) and fractional shortening (FS) were slightly increased, cardiac output was significantly reduced (Fig. 2A and D). Pulsed Doppler and tissue Doppler echocardiography further demonstrated diastolic dysfunction, characterized by a decreased E/A ratio and an increased E/e' ratio (Fig. 2B). Mice after BDL also exhibited significant reductions in both distance and time on the treadmill exercise test (Fig. 2C). Severe hemodynamic abnormalities were observed, including reductions in systolic blood pressure, diastolic blood pressure, and mean arterial pressure (Fig. 2D). Furthermore, electrocardiograms showed prolonged corrected QT (QTc) and QRS intervals. QTc increased most prominently at two weeks, then declined at four to eight weeks, but remained significantly elevated compared with controls (Supplementary Fig. 1A). Together, these findings demonstrate that mice subjected to BDL develop significant impairment of cardiac function.

BDL-induced cardiac damage in mice

We next examined the cardiac pathology and physiology of mice subjected to BDL. Serum analysis following BDL indicated the onset of cardiomyopathy. Markers of myocardial injury, including creatine kinase and creatine kinase-MB, gradually decreased from two to eight weeks after BDL. In contrast, brain natriuretic peptide (BNP), its precursor N-terminal pro-B-type natriuretic peptide, and cardiac troponin I increased significantly at two weeks post-surgery, then declined at four and eight weeks but remained elevated compared with controls, indicating persistent myocardial injury (Fig. 3A). Heart weight and heart-to-tibia length ratio were significantly reduced in mice subjected to BDL compared with controls (Fig. 3B), and reduced heart vol-

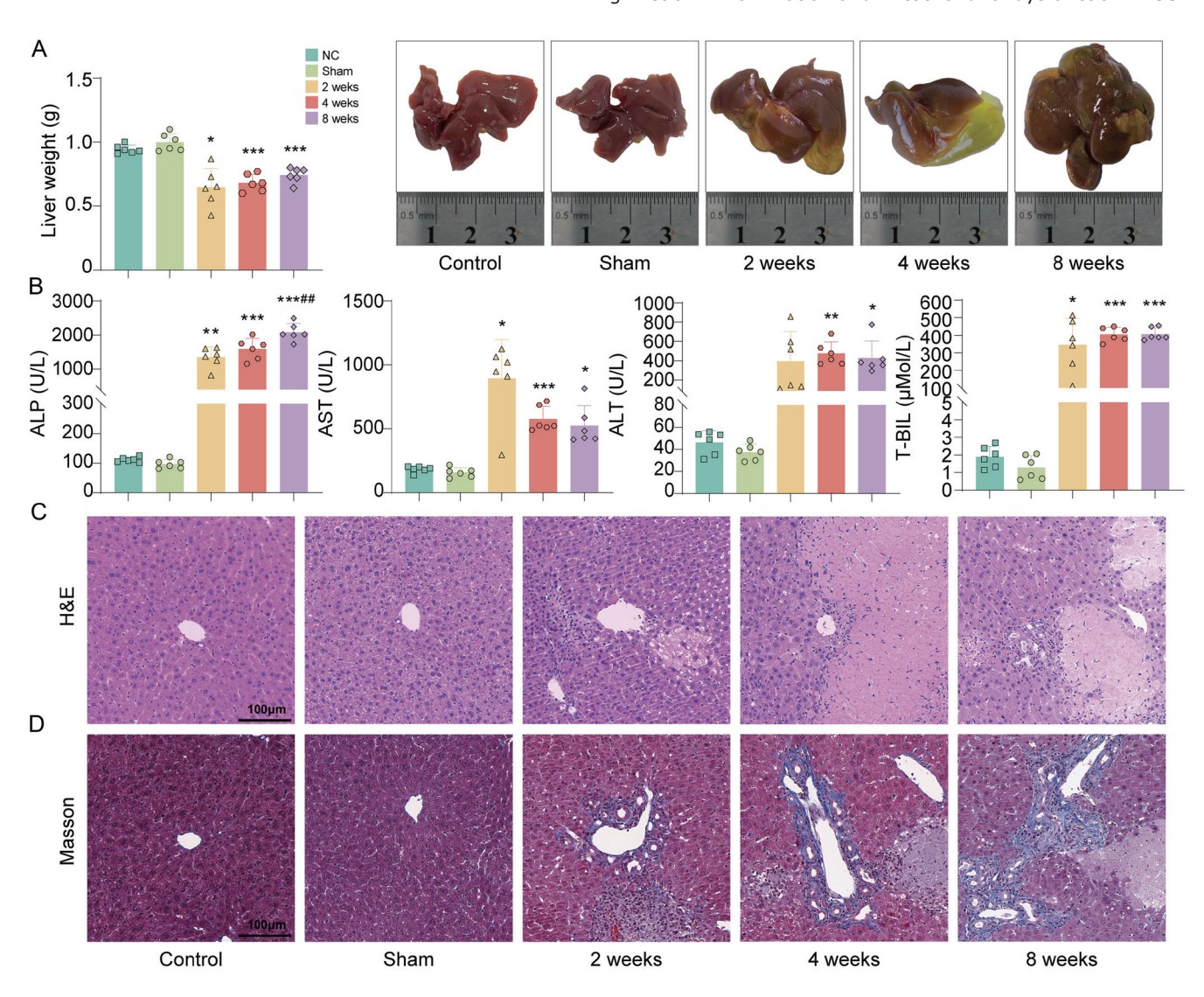


Fig. 1. Dynamic effects of bile duct ligation on bile duct response and liver injury in mice. (A) Mouse liver weight and liver appearance; (B) Serum alkaline phosphatase, aspartate aminotransferase, alanine aminotransferase, and total bilirubin levels; (C) Hematoxylin and eosin staining to observe liver pathological damage; (D) Masson staining to observe liver fibrosis (n = 6). Analytical data are expressed as mean \pm SEM. *p < 0.05, **p < 0.01, ***p < 0.001 vs. Control group; ##p < 0.01 vs. two weeks group. ALP, alkaline phosphatase; AST, aspartate aminotransferase; ALT, alanine aminotransferase; T-BIL, total bilirubin; H&E, hematoxylin and eosin.

ume was further confirmed by morphological analysis (Fig. 3C). Wheat germ agglutinin staining showed that myocardial cell diameter decreased progressively, with reductions beginning at two weeks and becoming more pronounced at four weeks (Fig. 3D). These findings suggest that CCM induces ventricular remodeling, characterized primarily by myocardial atrophy. Histological evaluation supported these observations. Hematoxylin and eosin staining demonstrated that myocardial cells in controls were tightly and orderly arranged, with evenly stained cytoplasm and clearly defined nuclei. In contrast, myocardial fibers in mice with CCM were hypertrophic, thickened, and loosely and irregularly arranged, with enlarged intercellular spaces, variable nuclear size, and occasional nuclear fusion. Inflammatory cell infiltration was markedly increased, with clusters surrounding blood vessels and extending into adjacent tissues (Fig. 3E).

BDL-induced myocardial apoptosis and fibrosis in mice

Protein expression analysis of Bax, Bcl-2, and caspase-3

demonstrated that cardiomyocytes in mice with CCM underwent apoptosis, with minimal apoptosis at two weeks, significant apoptosis at four weeks, and further increases at eight weeks (Fig. 4A). TUNEL staining confirmed progressive myocardial apoptosis (Fig. 4B). Masson's trichrome and Sirius Red staining revealed abundant collagen fiber deposition in the interstitial and perivascular regions of the myocardium in mice subjected to BDL. Fibrosis was mild at two to four weeks but became more pronounced by eight weeks (Fig. 4C and D). RT-qPCR analysis showed that the expression of fibrosis markers a-smooth muscle actin, collagen type I alpha 1, and transforming growth factor- $\beta 1$ progressively increased over time after BDL (Fig. 4E). These findings indicate that myocardial fibrosis is a key contributor to the development of CCM.

BDL-induced myocardial inflammation in mice

Inflammation plays a crucial role in cardiac injury; therefore, we further examined inflammatory factors in mice

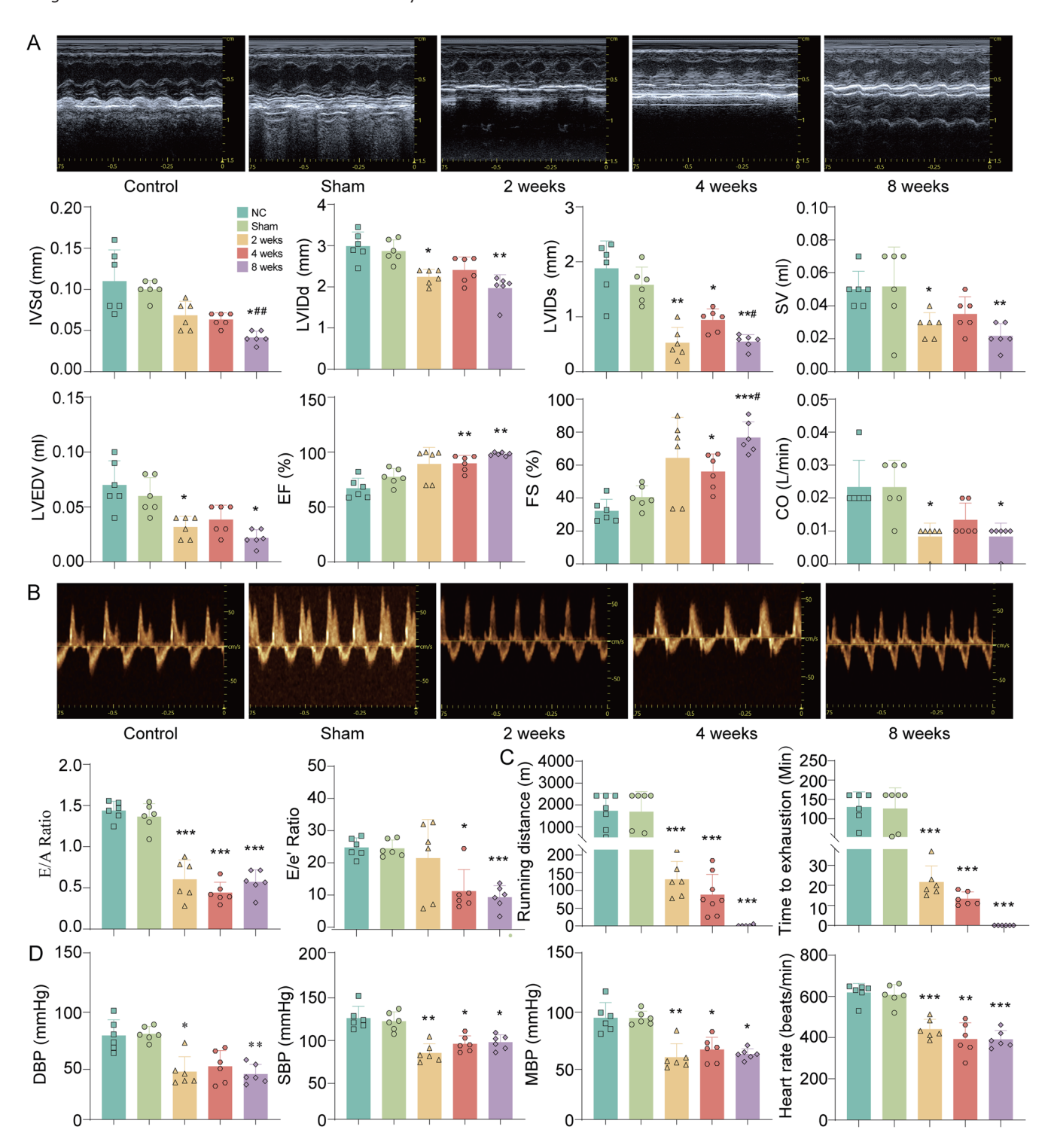


Fig. 2. Dynamic effects of bile duct ligation on cardiac function and exercise performance in mice. (A) Mouse cardiac ultrasound and data analysis; (B) E/A and E/e' ratios to evaluate the diastolic function of bile duct ligation mice; (C) Mouse treadmill exercise data analysis; (D) Analysis of blood pressure data of mice (n = 6). Analytical data are expressed as mean \pm SEM. *p < 0.05, **p < 0.01, ***p < 0.01 vs. Control group; *p < 0.05, **p < 0.01 vs. two weeks group. IVSd, interventricular stell thickness; LVIDd, left ventricular internal diameter systole; SV, stroke volume; LVEDV, left ventricular end-diastolic volume; EF, ejection fraction; FS, fractional shortening; CO, cardiac output; DBP, diastolic blood pressure; SBP, systolic blood pressure; MBP, mean arterial pressure.

subjected to BDL. Gene expression analysis showed significantly higher levels of IL-1 β , IL-6, p65, and TNF in myocardial tissue, with TNF expression peaking at two weeks and

declining slightly at four weeks (Fig. 5A). Consistently, immunohistochemistry revealed markedly elevated levels of $IL-1\beta$, IL-6, p65, and TNF in myocardial tissue, indicating

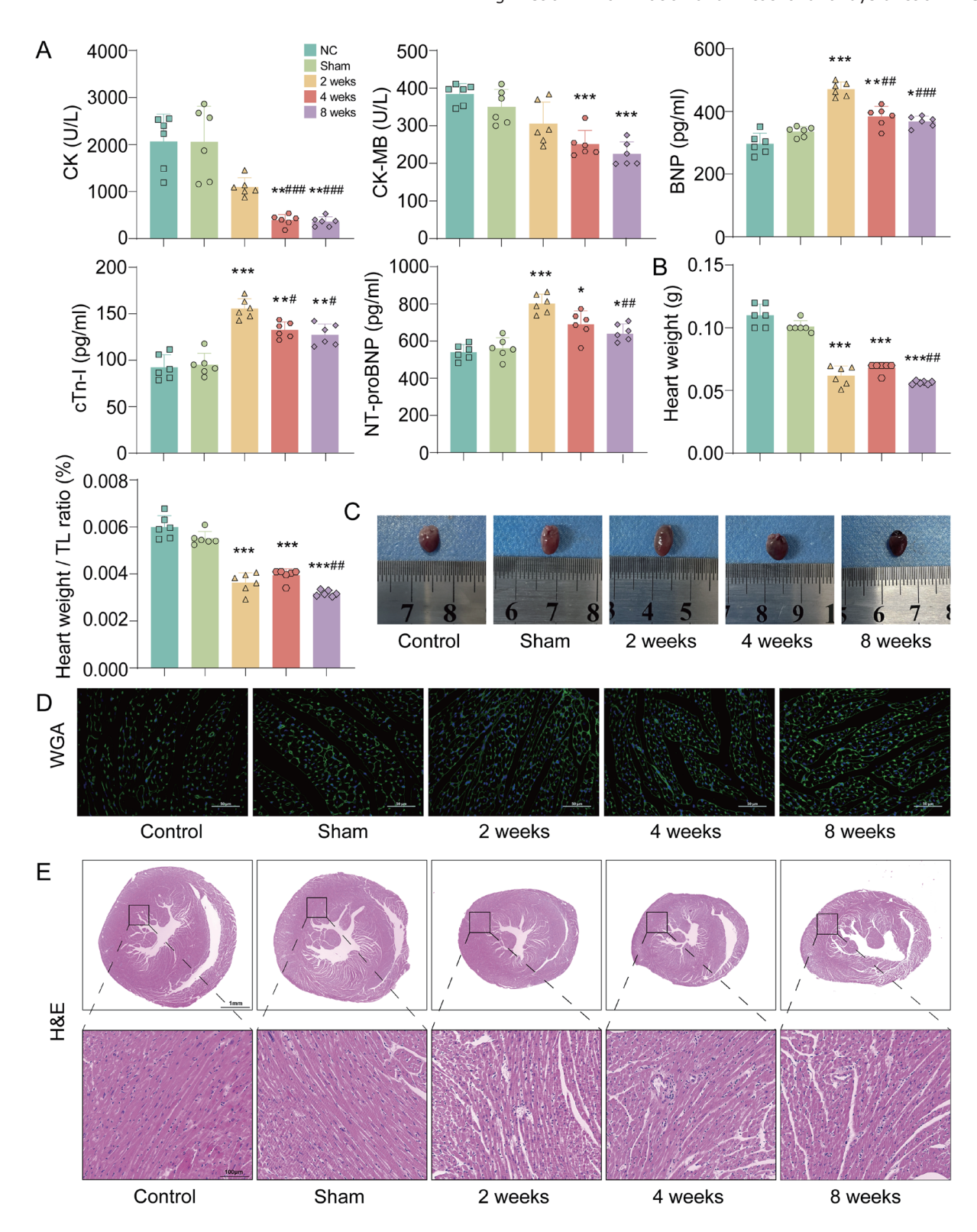


Fig. 3. Dynamic effects of bile duct ligation on heart weight, cardiomyocyte morphology, and ventricular remodeling in mice. (A) Serum levels of creatine kinase, creatine kinase-MB, brain natriuretic peptide, its precursor N-terminal pro-B-type natriuretic peptide, and cardiac troponin I; (B) Ratio of heart weight to tibia length in BDL-induced mice; (C) Appearance of the heart in BDL-induced mice; (D) Wheat germ agglutinin staining used to observe cardiac cell morphology; (E) Hematoxylin and eosin staining used to observe cardiac pathological damage (n = 3 or 6). Analytical data are presented as mean \pm SEM. "p < 0.05, **p < 0.01, ***p < 0.01, ***p

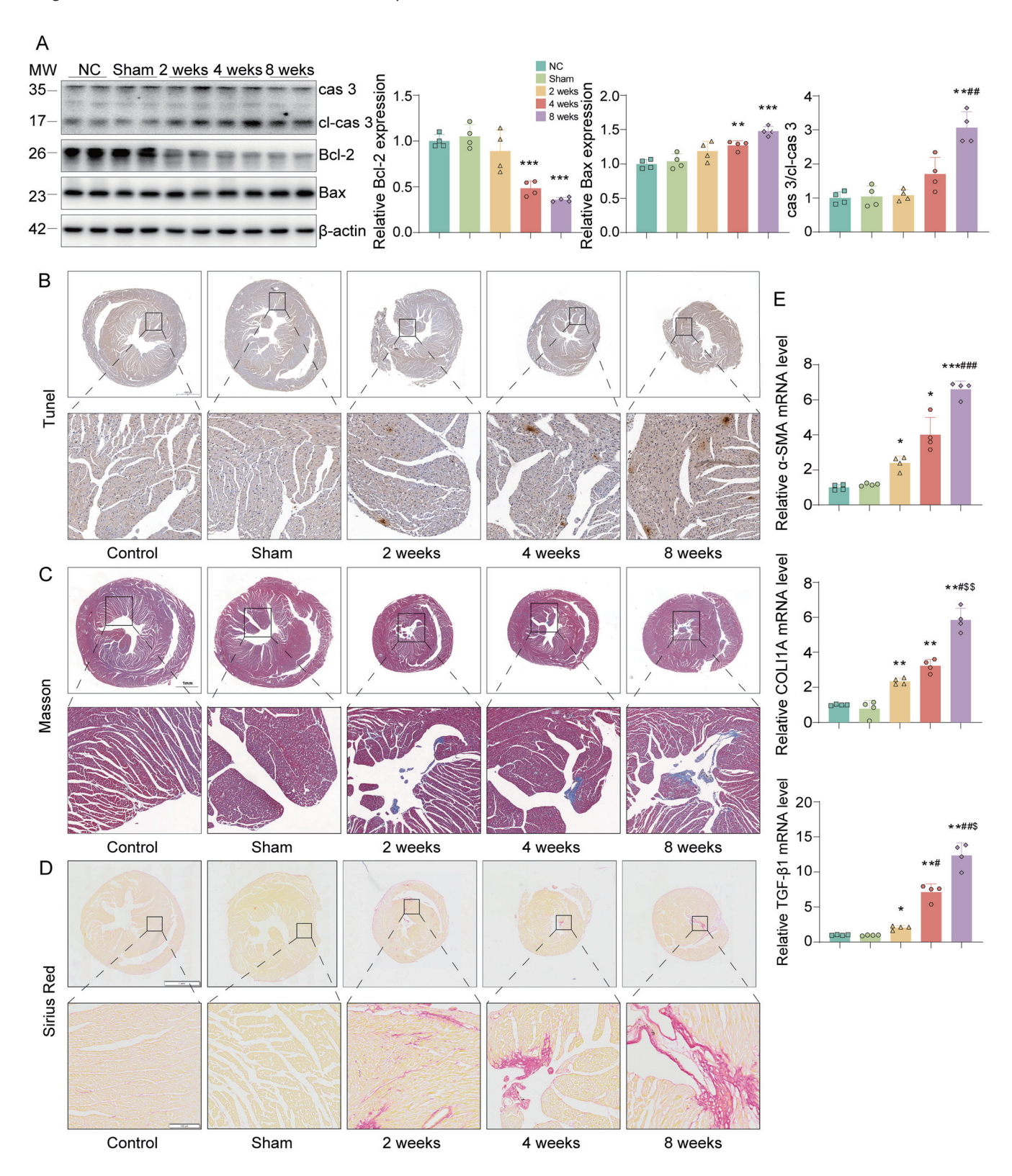


Fig. 4. Dynamic effects of bile duct ligation on myocardial injury, apoptosis, and fibrosis in mice. (A) Western blot used to detect the expression of apoptosis-related indicators Bax, Bcl-2, and caspase-3 in cardiac tissue; (B) TUNEL staining to observe apoptosis; (C) Masson staining used to observe cardiac fibrosis; (D) Sirius Red staining used to observe cardiac fibrosis; (E) RT-qPCR used to analyze the mRNA expression of fibrosis markers α-smooth muscle actin, collagen type I alpha 1, and transforming growth factor-β1 in cardiac tissue (n = 3). The analyzed data are presented as mean \pm SEM. *p < 0.05, **p < 0.01, ***p < 0.01, *

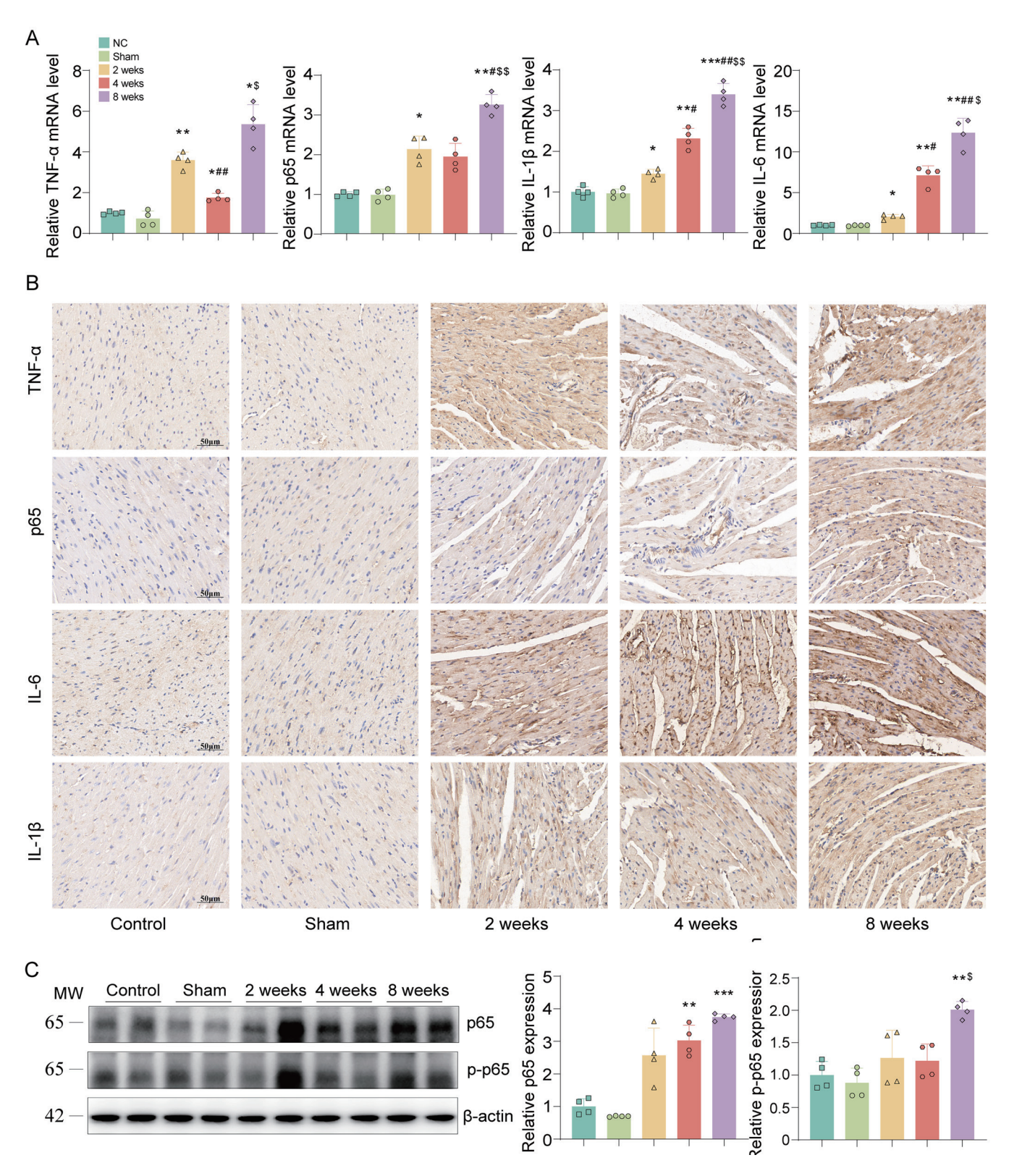


Fig. 5. Dynamic effects of bile duct ligation on myocardial inflammation in mouse hearts. RT-qPCR used to quantify the mRNA expression of inflammatory markers tumor necrosis factor, p65, interleukin-1 β , and interleukin-6 in cardiac tissue; (B) Immunohistochemistry used to detect the expression of cardiac inflammatory markers tumor necrosis factor, p65, interleukin-1 β , and interleukin-6 in bile duct ligation-induced mice; (C) Western blotting used to detect inflammation-related proteins in cirrhotic cardiomyopathy, specifically focusing on p65 and phosphorylated p65 (n = 3 or 4). Analytical data are expressed as mean \pm SEM. *p < 0.05, **p < 0.01, ***p < 0.001 vs. Control group; *p < 0.05, **p < 0.01 vs. four weeks group. MW, molecular weight.

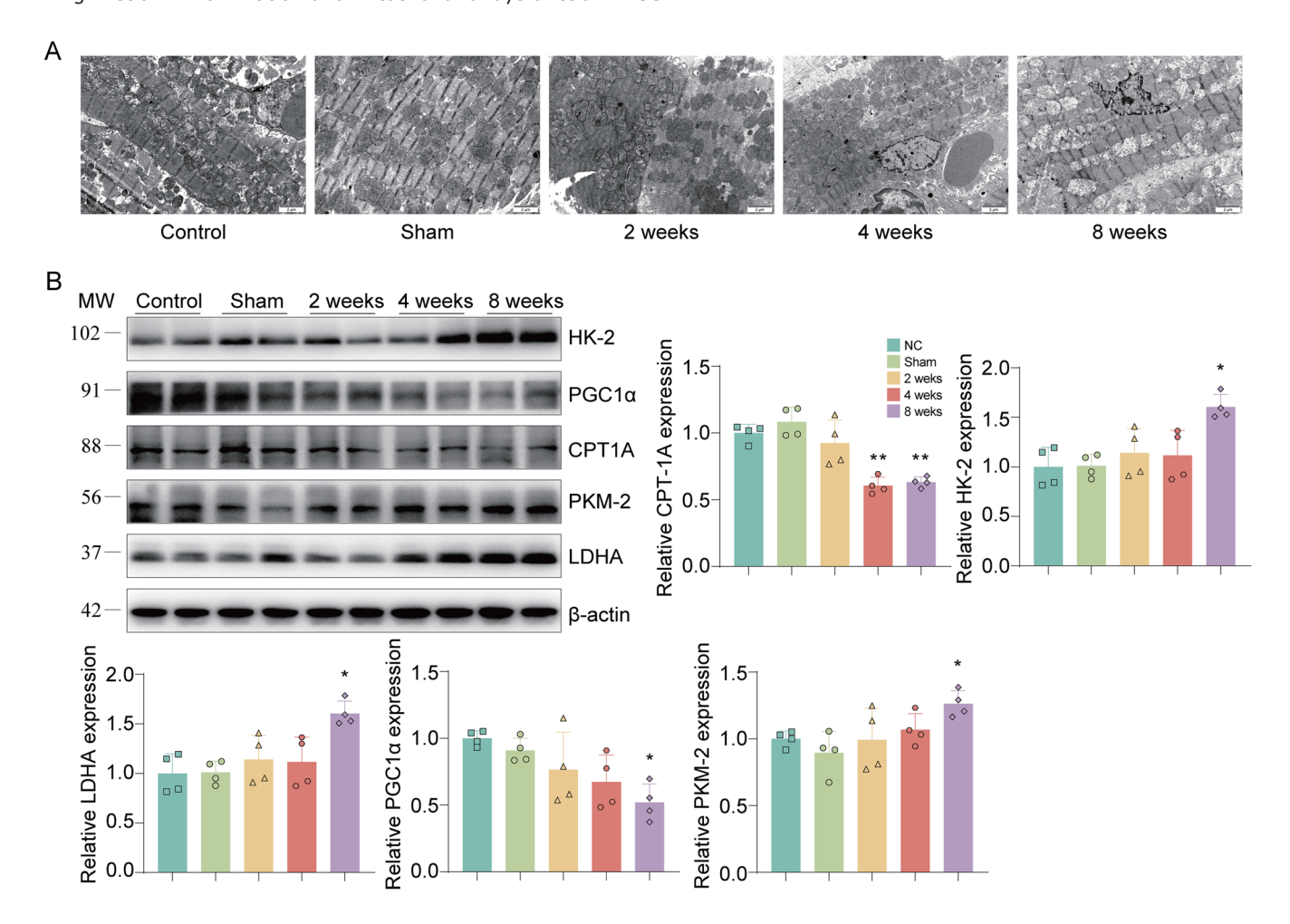


Fig. 6. Dynamic effects of bile duct ligation on mitochondrial injury and autophagy in mouse hearts. Electron microscopy observation of mitochondrial morphology; (B) Western blot analysis of mitochondrial-related proteins carnitine palmitoyltransferase 1A, peroxisome proliferator-activated receptor alpha, lactate dehydrogenase A, hexokinase 2, and pyruvate kinase M2 expression (n = 3 or 4). Analytical data are expressed as mean \pm SEM. *p < 0.05, **p < 0.01 vs. Control group. MW, molecular weight.

increased inflammatory cell infiltration (Fig. 5B). Western blotting further confirmed upregulated expression of phosphorylated p65 and total p65 proteins, supporting the involvement of inflammatory signaling pathways in the pathogenesis of CCM (Fig. 5C).

BDL-induced cardiac mitochondrial dysfunction in mice

Given that the heart is the most energy-demanding organ in the body, we investigated mitochondrial alterations in the hearts of mice subjected to BDL. Morphological examination revealed cardiomyocyte edema, widened nuclear spaces, nuclear condensation, mitochondrial swelling, and cristae rupture at two weeks. By eight weeks, mitochondrial damage had further progressed, with persistent swelling and rupture (Fig. 6A). Western blot analysis demonstrated a progressive decline in peroxisome proliferator-activated receptor alpha, a marker of mitochondrial biogenesis, as well as CPT1A, a key enzyme in fatty acid β -oxidation, from two to eight weeks post-surgery. In contrast, the expression of glycolytic enzymes, including hexokinase 2, PKM2, and LDHA, was significantly increased in the hearts of mice with CCM. These findings indicate that BDL induces severe mitochondrial injury in the heart, characterized by reduced β -oxidation and

enhanced glycolysis, suggesting a metabolic shift from fatty acid β -oxidation to glycolysis (Fig. 6B).

Cardiac dysfunction in patients with cirrhosis

Compared with healthy controls, patients with cirrhosis showed significantly elevated liver function markers, including aspartate aminotransferase, alkaline phosphatase, alanine aminotransferase, total bile acid, total bilirubin, and lactate dehydrogenase (Fig. 7A). Echocardiographic analysis demonstrated significant increases in end-diastolic interventricular septal thickness, end-diastolic left ventricular posterior wall thickness, and left atrial diameter, whereas no significant differences were observed in EF or FS, suggesting myocardial hypertrophy or dilation in these patients (Fig. 7B). The 65 patients with cirrhosis were then classified into two groups: compensated cirrhosis and decompensated cirrhosis. Patients with decompensated cirrhosis had significantly higher total bilirubin, total bile acid, and BNP levels compared with those in the compensated cirrhosis group (Fig. 7C). Echocardiographic parameters, including aortic root diameter, left ventricular diameter, and left atrial diameter, were also significantly elevated in the decompensated cirrhosis group, whereas EF and FS did not differ significantly (Fig. 7D). Correlation analysis showed that total bilirubin and

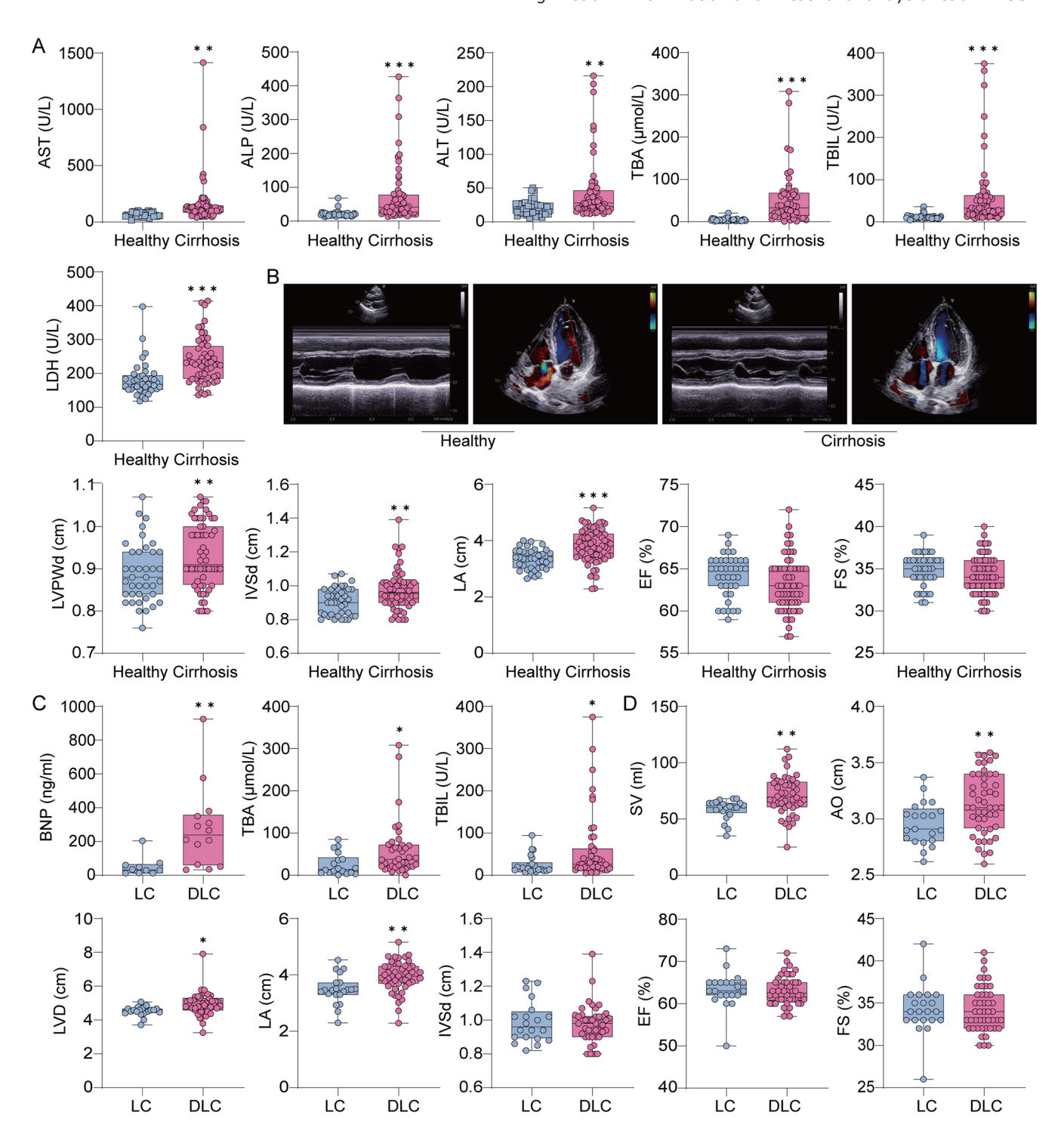


Fig. 7. Cardiac dysfunction in patients with cirrhosis. (A) Serum liver function indexes in patients with cirrhosis; (B) Cardiac ultrasound and data analysis in patients with cirrhosis (Healthy = 39, Cirrhosis = 65); (C) Serum analysis in patients with liver cirrhosis (LC) and decompensated liver cirrhosis (DLC); (D) Ultrasound analysis in patients with liver cirrhosis (LC) and decompensated liver cirrhosis (LC) and decompensated liver cirrhosis (DLC) (LC = 19, DLC = 45). Analytical data are expressed as mean \pm SEM. $^*p < 0.05$, $^{**}p < 0.01$, $^{***}p < 0.01$, $^{**}p < 0.01$, aspartate aminotransferase; ALP, alkaline phosphatase; ALT, alanine aminotransferase; TBA, total bilirubin; LDH, lactate dehydrogenase; LVPWd, left ventricular posterior wall diameter; IVSd, interventricular setal thickness; LA, left atrium; EF, ejection fraction; FS, fractional shortening; BNP, brain natriuretic peptide; SV, stroke volume; AO, aorta; LVD, left ventricular dimension; IVSd, interventricular septalt hickness.

total bile acid were positively associated with BNP, QT, QTc, SV, left ventricular diameter, left atrial diameter, and aortic root diameter, and negatively associated with EF and FS.

These findings indicate that the extent of cardiac dysfunction in patients with cirrhosis is closely linked to disease severity (Supplementary Tables 2 and 3).

Discussion

Echocardiography is considered the most reliable method for assessing cardiac function in CCM. In this study, echocardiography was first performed to evaluate cardiac performance in mice. The E/A ratio reflects left ventricular inflow velocity during early rapid passive filling (E-wave) and atrial contraction (A-wave); in diastolic dysfunction, the E/A ratio falls below 1. Furthermore, the E/e' ratio serves as an indicator of left ventricular filling pressure and is less dependent on loading conditions in the presence of diastolic dysfunction. As diastolic function deteriorates, e' decreases and the E/e' ratio increases. 14,15 Shahvaran et al. summarized echocardiographic data from 615 patients with cirrhosis and reported that the mean E/A ratio and mean left ventricular EF were significantly lower in patients with cirrhosis than in healthy controls. 16 In our BDL mouse model, the E/A ratio was consistent with that observed in patients with cirrhosis, although the left ventricular EF in mice subjected to BDL was slightly higher than that in controls. This finding contrasts with the 2020 diagnostic criteria for CCM established by the Cirrhotic Cardiomyopathy Consortium, which define systolic dysfunction as an EF < 50%. EF, a key afterload-dependent parameter, is the ratio of SV to end-diastolic volume. The increase in FF values observed in our study may reflect a smaller reduction in SV relative to the decrease in end-diastolic volume. Indeed, several murine studies have reported preserved or even increased EF in CCM. 7,17-19 Likewise, clinical studies suggest that CCM is often characterized by diastolic dysfunction and preserved systolic function at rest, with normal or elevated EF.20-22 Bushyhead et al. further reported that increased EF is associated with worse outcomes in cirrhosis.²³ In our clinical cohort, increased end-diastolic left ventricular posterior wall thickness, end-diastolic interventricular septal thickness, and left atrial diameter, together with unchanged EF and FS, indicated impaired diastolic function with preserved systolic function, findings that align with previous research. We hypothesize that this discrepancy may reflect the heterogeneous phenotypes of CCM. CCM develops gradually, progressing from a compensated to a decompensated state, and typically manifests as chronic cardiac dysfunction with myocardial hypertrophy, systolic or diastolic impairment, and electrophysiological abnormalities. Myocardial hypertrophy, induced by increased cardiac load, represents a compensatory mechanism. However, the BDL mouse model is relatively acute, inducing CCM over a short timeframe without allowing for the development of long-term compensatory hypertrophy. In our study, heart weight decreased, myocardial cells underwent atrophy, and end-diastolic left ventricular internal diameter, end-systolic left ventricular internal diameter, and left ventricular end-diastolic volume all declined. Consequently, myocardial atrophy and reduced ventricular volume contributed to an increased rather than decreased EF.

We monitored blood pressure in mice and observed hypotension following BDL surgery. In patients with cirrhosis, alterations in liver structure and metabolic function increase intrahepatic vascular resistance and cause portal hypertension. Portal hypertension, ²⁴ together with arterial vasodilation, results in central hypovolemia, which in turn leads to hypotension, activation of a hyperdynamic circulatory state, and stimulation of potent vasoconstrictor systems. These hemodynamic changes contribute to complications such as CCM. ²⁵ Our study showed that BDL induces electrocardiographic abnormalities, most notably prolongation of the QTC interval. The QT interval on the electrocardiogram represents the time from the onset of the QRS complex to the end of the T wave, reflecting the total duration of ventricular depolarization and repolarization, which generally corresponds to

ventricular contraction during systole. Because the QT interval is influenced by heart rate, the QTc interval is commonly used to determine whether QT prolongation is present. A prolonged QTc interval reflects slowed depolarization and increased action potential duration. Potential duration, 30% – 70% of patients with cirrhosis present with prolonged QT intervals, highlighting the importance of monitoring the QTc interval in patients with CCM.

In our study, mice with CCM showed increased circulating cardiac biomarkers, including BNP, N-terminal pro-B-type natriuretic peptide, and cardiac troponin I, indicating potential cardiac dysfunction. BNP and N-terminal pro-B-type natriuretic peptide, secreted by the ventricles, are elevated in both compensated and decompensated cirrhosis in response to myocardial damage and hypertrophy. ^{28,29} Cardiac troponin I is a key marker of myocardial damage and is elevated in some patients with cirrhosis, who often exhibit subclinical myocardial injury, such as reduced SV and left ventricular mass index. ³⁰ These findings are consistent with our observations.

The results of this study clearly demonstrate that CCM is associated with myocardial fibrosis and apoptosis, both of which play central roles in cardiac dysfunction. Masson's trichrome staining revealed collagen fiber accumulation in the myocardial interstitium and perivascular regions, indicating structural alterations secondary to chronic liver disease. Fibrosis increases myocardial stiffness, impairing both systolic and diastolic function. RT-qPCR results showed progressive upregulation of fibrotic markers, such as a-smooth muscle actin, collagen type I alpha 1, and transforming growth factor-β1, from two to eight weeks after BDL surgery, reflecting worsening fibrosis over time. This accumulation disrupts normal myocardial architecture and function, leading to reduced contractility and increased cardiac workload in CCM. These findings are consistent with those of Isaak et al., who reported that myocardial fibrosis in cirrhosis correlates with systemic inflammation and the degree of cirrhosis on magnetic resonance imaging.31 Such structural changes exacerbate cardiac dysfunction.

Beyond fibrosis, cardiomyocyte apoptosis is a critical factor in the progression of CCM. In our study, pro-apoptotic markers such as Bax and caspase-3 were upregulated, whereas the anti-apoptotic protein Bcl-2 was downregulated, indicating enhanced cardiomyocyte apoptosis in mice subjected to BDL. The activation of apoptotic pathways in CCM may be driven by the chronic inflammatory state of cirrhosis. As cirrhosis advances, inflammatory cytokines and reactive oxygen species contribute to mitochondrial dysfunction and DNA damage, triggering cardiomyocyte apoptosis. This loss of cardiomyocytes reduces cardiac contractile capacity and further promotes myocardial fibrosis. Nam et al. also reported a link between apoptosis and cardiomyopathy in bile duct-ligated mice, showing that inhibition of apoptosis alleviated myocardial damage.4 The persistence of apoptosis in our CCM model suggests that therapeutic strategies targeting apoptotic pathways may help preserve myocardial function in patients with cirrhosis.

This study also showed that inflammatory cytokines, including IL-1 β , IL-6, IL-18, p65, and TNF, were significantly elevated following BDL, consistent with previous reports implicating inflammation in CCM. 32 The activation of p65 has been reported to play a major role in reducing cardiac contractility in CCM. 33 Moreover, oxidative stress and p65 activation enhance the production of proinflammatory mediators such as TNF and IL-1 β . In turn, excessive TNF stimulates p65 transcription and promotes oxidative stress in cardiomyocytes. 34 Studies have also demonstrated that TNF re-

duces cardiac contractility in mice subjected to BDL through the p65-inducible nitric oxide synthase and p38 mitogenactivated protein kinase signaling pathways. 35 These findings suggest that inhibiting TNF may improve cardiac contractility during systemic inflammation. In addition, inflammation-induced mitochondrial dysfunction can impair fatty acid oxidation and promote a glycolytic shift, thereby contributing to the progression of CCM.36

Although not traditionally classified as a metabolic organ, the heart is the most energy-demanding organ in the body. 37,38 Under normal conditions, 60%-90% of cardiac adenosine triphosphate is generated through fatty acid oxidation, with the remainder derived from pyruvate oxidation.³⁷ However, in pathological states, overt cardiac dysfunction is often associated with reduced fatty acid oxidation.³⁹⁻⁴² To assess whether this occurs in CCM, we examined the effects of BDL on fatty acid β-oxidation. CPT1A, the rate-limiting enzyme of β-oxidation in mitochondria, was significantly reduced in cardiac tissue from mice subjected to BDL. This finding suggests a link between impaired fatty acid oxidation and the development of CCM. Alterations in mitochondrial fission dynamics have been shown to disrupt cellular metabolism, 43 and mitochondrial fission is associated with a glycolytic metabolic profile.44 Consistent with this, we observed increased levels of glycolytic enzymes, including hexokinase 2 and PKM2, in the hearts of BDL-treated mice, indicating a metabolic shift toward glycolysis and activation of the Warburg effect, which is characterized by enhanced aerobic glycolysis and lactate production.45 Furthermore, PKM2 can translocate to the nucleus, induce the expression of glycolytic enzymes such as LDHA,46 and contribute to pro-apoptotic processes.47 In line with this, our study demonstrated increased expression of hexokinase 2, PKM2, and LDHA, suggesting that similar metabolic reprogramming occurs in the hearts of mice with CCM. These findings raise the possibility that targeted mitochondrial therapies may mitigate CCM-associated cardiac damage by improving myocardial energy metabolism. Vázquez-Abuín et al. reported that stimulation of soluble guanylate cyclase improved cardiac function and mitochondrial activity in a rat model of early-stage heart failure with preserved EF.48 Similarly, Moheimani et al. demonstrated that metformin and cyclosporine A exert cardioprotective effects in patients with liver cirrhosis through modulation of cardiac energy metabolism,⁴⁹ potentially by enhancing myocardial mitochondrial function.

Conclusions

Our results indicate that mice subjected to BDL develop progressive cardiac dysfunction, with fibrotic changes detectable as early as four weeks post-surgery. Inflammation and mitochondrial damage likely contribute significantly to this process, although the precise mechanisms require further investigation. In patients with cirrhosis, cardiac dysfunction is closely associated with disease severity, highlighting the importance of monitoring cardiac function and electrocardiograms in clinical practice. However, the EF values observed in BDL-treated mice did not align with the established diagnostic criteria for CCM in patients. This discrepancy is likely attributable to cardiac atrophy in these mice, whereas CCM in patients is typically characterized by myocardial hypertrophy and chamber dilation. Such differences should be taken into account in future mechanistic studies.

Acknowledgments

The authors thank the Center for Scientific Research of Anhui

Medical University for their valuable assistance in our experi-

Funding

This study was financially supported by grants from the National Natural Science Foundation of China (82174063, 82204703), the National Natural Science Foundation of Anhui Province (2008085MH287), and the Anhui Province Traditional Chinese Medicine Inheritance and Innovation Scientific Research Project (2020cczd03).

Author contributions

Study conception and design (CG, YS), study performance, data obtaining (YD), and data interpretation (CH, GY). All authors participated in drafting and revising the manuscript. All authors have approved the final version and publication of the manuscript.

Ethical statement

This study was approved by the Ethics Committee of Anhui Medical University, with animal study approval number LLSC20210241 and clinical study approval number PJ2024-05-76, and was conducted in accordance with the principles of the Declaration of Helsinki (as revised 2024). All animal received human care.

Data sharing statement

The data used to support the findings of this study are included within the article.

References

- Chayanupatkul M, Liangpunsakul S. Cirrhotic cardiomyopathy: review of pathophysiology and treatment. Hepatol Int 2014;8(3):308–315. doi:10.1007/s12072-014-9531-y, PMID:25221635.
 Chahal D, Liu H, Shamatutu C, Sidhu H, Lee SS, Marquez V. Review article: comprehensive analysis of cirrhotic cardiomyopathy. Aliment Pharmacol Ther 2021;53(9):985–998. doi:10.1111/apt.16305, PMID:33689169.
 Izzy M, VanWagner LB, Lin G, Altieri M, Findlay JY, Oh JK, et al. Redefining Cirrhotic Cardiomyopathy. All Pharatology 2020:21(1):334–10.
- Cirrhotic Cardiomyopathy for the Modern Era. Hepatology 2020;71(1):334 345. doi:10.1002/hep.30875, PMID:31342529.
- [4] Nam SW, Liu H, Wong JZ, Feng AY, Chu G, Merchant N, et al. Cardiomyo-cyte apoptosis contributes to pathogenesis of cirrhotic cardiomyopathy in bile duct-ligated mice. Clin Sci (Lond) 2014;127(8):519–526. doi:10.1042/CS20130642, PMID:24712830.
- Desai MS, Shabier Z, Taylor M, Lam F, Thevananther S, Kosters A, et al. Hypertrophic cardiomyopathy and dysregulation of cardiac energetics in a mouse model of biliary fibrosis. Hepatology 2010;51(6):2097–2107. doi:10.1002/hep.23585, PMID:20512997.
- [6] Bátkai S, Mukhopadhyay P, Harvey-White J, Kechrid R, Pacher P, Kunos G. Endocannabinoids acting at CB1 receptors mediate the cardiac contractile dysfunction in vivo in cirrhotic rats. Am J Physiol Heart Circ Physiol 2007;293(3):H1689-H1695. doi:10.1152/ajpheart.00538.2007, PMID:17557913.
- PMID:1755/913.

 Matyas C, Erdelyi K, Trojnar E, Zhao S, Varga ZV, Paloczi J, et al. Interplay of Liver-Heart Inflammatory Axis and Cannabinoid 2 Receptor Signaling in an Experimental Model of Hepatic Cardiomyopathy. Hepatology 2020;71(4):1391–1407. doi:10.1002/hep.30916, PMID:31469200.
- [8] Uhlig M, Hein M, Habigt MA, Tolba RH, Braunschweig T, Helmedag MJ, et al. Cirrhotic Cardiomyopathy Following Bile Duct Ligation in Rats-A Matter of Time? Int J Mol Sci 2023;24(9):8147. doi:10.3390/ijms24098147, PMID:37175858.
- PMID: 37175858.
 Zeng Z, Lei Y, Yang C, Wu X, Zhang L, Yang Z, et al. The Therapeutic Effects of Baicalein on the Hepatopulmonary Syndrome in the Rat Model of Chronic Common Bile Duct Ligation. J Clin Transl Hepatol 2024;12(5):496–504. doi:10.14218/JCTH.2023.00513, PMID:38779522.
 Jiang M, Huang C, Wu Q, Su Y, Wang X, Xuan Z, et al. Sini San ameliorates CCI4-induced liver fibrosis in mice by inhibiting AKT-mediated hepatocyte apoptosis. J Ethnopharmacol 2023;303:115965. doi:10.1016/j. jep.2022.115965, PMID:36460296.
 Hai Y, Ma Q, Liu Z, Li D, Huang A, Zhu Y, et al. Oxidative stress-related biomarkers in thyroid eve disease: evidence from bioinformatics analysis and
- markers in thyroid eye disease: evidence from bioinformatics analysis and experimental validation. Front Immunol 2025;16:1635712. doi:10.3389/ fimmu.2025.1635712, PMID:40901474.

- [12] Hao H, Cao L, Jiang C, Che Y, Zhang S, Takahashi S, et al. Farnesoid X Receptor Regulation of the NLRP3 Inflammasome Underlies Cholestasis-Associated Sepsis. Cell Metab 2017;25(4):856–867.e5. doi:10.1016/j.
- cmet.2017.03.007, PMID:28380377.

 [13] Fuenzalida B, Yañez MJ, Mueller M, Mistry HD, Leiva A, Albrecht C. Evidence for hypoxia-induced dysregulated cholesterol homeostasis in preeclampsia: Insights into the mechanisms from human placental cells and tissues. FASEB J 2024;38(2):e23431. doi:10.1096/fj.202301708RR, PMID: 38265294.
- [14] Kasner M, Westermann D, Steendijk P, Gaub R, Wilkenshoff U, Weitmann K, et al. Utility of Doppler echocardiography and tissue Doppler imaging in the estimation of diastolic function in heart failure with normal ejection fraction: a comparative Doppler-conductance catheterization study. Circulation 2007;116(6):637–647. doi:10.1161/CIRCULATIONAHA.106.661983, PMID:17646587
- [15] Nagueh SF, Appleton CP, Gillebert TC, Marino PN, Oh JK, Smiseth OA, et al. Recommendations for the evaluation of left ventricular diastolic function by echocardiography. J Am Soc Echocardiogr 2009;22(2):107–133. doi:10.1016/j.echo.2008.11.023, PMID:19187853.
- [16] Shahvaran SA, Menyhárt O, Csedrik L, Patai ÁV. Diagnosis and Prevalence of Cirrhotic Cardiomyopathy: A Systematic Review and Meta-analysis. Curr Probl Cardiol 2021;46(10):100821. doi:10.1016/j.cpcardiol.2021.100821, PMID:34016482.
- [17] Pagourelias ED, Sotiriou P, Papadopoulos CE, Cholongitas E, Giouleme O, Vassilikos V. Left Ventricular Myocardial Mechanics in Cirrhosis: A Speckle Tracking Echocardiographic Study. Echocardiography 2016;33(2):223–232. doi:10.1111/echo.13010, PMID:26174780.
- [18] Padillo J, Rioja P, Muñoz-Villanueva MC, Vallejo JA, Ciria R, Muntane J,
- [18] Padilio J, Rioja P, Munoz-Villandeva MC, Vallejo JA, Ciria K, Muntane J, et al. BNP as marker of heart dysfunction in patients with liver cirrhosis. Eur J Gastroenterol Hepatol 2010;22(11):1331–1336. doi:10.1097/MEG.0b013e32833e6b2a, PMID:20729741.
 [19] Larsen GR, Henson K, Blue Y. Variants of human tissue-type plasminogen activator. Fibrin binding, fibrinolytic, and fibrinogenolytic characterization of genetic variants lacking the fibronectin finger-like and/or the epidermal growth factor domains. J Biol Chem 1988;263(2):1023–1029. PMID:3121618.
 [20] Shin WI, Song JC, Jun JC, Mon YJ, Kung HM, Jung K, et al. Effect of
- [20] Shin WJ, Song JG, Jun IG, Moon YJ, Kwon HM, Jung K, et al. Effect of ventriculo-arterial coupling on transplant outcomes in cirrhotics: Analysis of pressure-volume curve relations. J Hepatol 2017;66(2):328–337. doi:10.1016/j.jhep.2016.09.009, PMID:27686680. [21] Nazar A, Guevara M, Sitges M, Terra C, Solà E, Guigou C, *et al.* LEFT ven-
- tricular function assessed by echocardiography in cirrhosis: relationship to systemic hemodynamics and renal dysfunction. J Hepatol 2013;58(1):51– 57. doi:10.1016/j.jhep.2012.08.027, PMID:22989573.
 [22] Wong F, Liu P, Lilly L, Bomzon A, Blendis L. Role of cardiac structural and
- functional abnormalities in the pathogenesis of hyperdynamic circulation and renal sodium retention in cirrhosis. Clin Sci (Lond) 1999;97(3):259– 267. PMID:10464050.
- [23] Bushyhead D, Kirkpatrick JN, Goldberg D. Pretransplant echocardiograph-ic parameters as markers of posttransplant outcomes in liver transplant recipients. Liver Transpl 2016;22(3):316-323. doi:10.1002/lt.24375, MID:26609681.
- [24] Schwabl P, Seeland BA, Riedl F, Schubert TL, Königshofer P, Brusilovskaya K, et al. Splenectomy ameliorates portal pressure and anemia in animal models of cirrhotic and non-cirrhotic portal hypertension. Adv Med Sci 2022;67(1):154–162. doi:10.1016/j.advms.2022.02.005, PMID:35272246. [25] Wiese S, Hove JD, Bendtsen F, Møller S. Cirrhotic cardiomyopathy: pathogenesis and clinical relevance. Nat Rev Gastroenterol Hepatol
- 2014;11(3):177–186. doi:10.1038/nrgastro.2013.210, PMID:24217347.

 [26] Karmakar S, Padman A, Swamy Mane N, Sen T. Hypokalemia: a potent risk for QTc prolongation in clarithromycin treated rats. Eur J Pharmacol
- 2013;709(1-3):80-84. doi:10.1016/j.ejphar.2013.03.038, PMID:33567068.

 [27] Lee W, Vandenberk B, Raj SR, Lee SS. Prolonged QT Interval in Cirrhosis: Twisting Time? Gut Liver 2022;16(6):849-860. doi:10.5009/gnl210537, PMID:35864808.
- [28] Wang LK, An XF, Wu XL, Zhang SM, Yang RM, Han C, et al. Doppler myo-cardial performance index combined with plasma B-type natriuretic pepcardial performance index combined with plasma B-type natriuretic peptide levels as a marker of cardiac function in patients with decompensated cirrhosis. Medicine (Baltimore) 2018;97(48):e13302. doi:10.1097/MD.0000000000013302, PMID:30508917.

 [29] Loomba R, Adams LA. The 20% Rule of NASH Progression: The Natural History of Advanced Fibrosis and Cirrhosis Caused by NASH. Hepatology 2019;70(6):1885–1888. doi:10.1002/hep.30946, PMID:31520407.

 [30] Kumar S, Griffith N, Walter D, Swett M, Raman V, Vargas JD, et al. Characteristics of Mecandial Livius With Nick Societishis Topology. Placet Inches
- terization of Myocardial Injury With High-Sensitivity Troponin. Tex Heart Inst

- J 2023;50(6):e238108. doi:10.14503/THIJ-23-8108, PMID:38115713.
- J 2023;50(6):e238108. doi:10.14503/IHIJ-23-8108, PMID:38115/13.

 [31] Isaak A, Praktiknjo M, Jansen C, Faron A, Sprinkart AM, Pieper CC, et al. Myocardial Fibrosis and Inflammation in Liver Cirrhosis: MRI Study of the Liver-Heart Axis. Radiology 2020;297(1):51–61. doi:10.1148/radiol.20202020157, PMID:32808886.

 [32] Wiese S, Mortensen C, Gøtze JP, Christensen E, Andersen O, Bendtsen F, et al. Cardiac and proinflammatory markers predict prognosis in cirrhosis. Liver Int 2014;34(6):e19–e30. doi:10.1111/liv.12428, PMID:24313898.
- [33] Bernardi M, Moreau R, Angeli P, Schnabl B, Arroyo V. Mechanisms of de-compensation and organ failure in cirrhosis: From peripheral arterial vaso-
- dilation to systemic inflammation hypothesis. J Hepatol 2015;63(5):1272–1284. doi:10.1016/j.jhep.2015.07.004, PMID:26192220.

 [34] de Almeida AJPO, de Almeida Rezende MS, Dantas SH, de Lima Silva S, de Oliveira JCPL, de Lourdes Assunção Araújo de Azevedo F, et al. Unveiling the Role of Inflammation and Oxidative Stress on Age-Related Cardiovascular Diseases. Oxid Med Cell Longev 2020;2020:1954398. doi:10.1155/2020/1954398, PMID:32454933.
- [35] Yang YY, Liu H, Nam SW, Kunos G, Lee SS. Mechanisms of TNFalpha-in-duced cardiac dysfunction in cholestatic bile duct-ligated mice: interaction between TNFalpha and endocannabinoids. J Hepatol 2010;53(2):298-306. doi:10.1016/j.jhep.2010.03.011, PMID:20626112.
- [36] Niaz Q, Tavangar SM, Mehreen S, Ghazi-Khansari M, Jazaeri F. Evaluation of statins as a new therapy to alleviate chronotropic dysfunction in cirrhotic rats. Life Sci 2022;308:120966. doi:10.1016/j.lfs.2022.120966, PMID:36150464.
- [37] Stanley WC, Recchia FA, Lopaschuk GD. Myocardial substrate metabolism in the normal and failing heart. Physiol Rev 2005;85(3):1093–1129. doi:10.1152/physrev.00006.2004, PMID:15987803.
- [38] Carley AN, Taegtmeyer H, Lewandowski ED. Matrix revisited: mechanisms linking energy substrate metabolism to the function of the heart. Circ Res 2014;114(4):717-729. doi:10.1161/CIRCRESAHA.114.301863, PMID:24526677.
- [39] Osorio JC, Stanley WC, Linke A, Castellari M, Diep QN, Panchal AR, et al. Impaired myocardial fatty acid oxidation and reduced protein expression of retinoid X receptor-alpha in pacing-induced heart failure. Circulation 2002;106(5):606-612. doi:10.1161/01.cir.0000023531.22727.c1, PMID:12147544.
- [40] Heather LC, Cole MA, Lygate CA, Evans RD, Stuckey DJ, Murray AJ, et al. Fatty acid transporter levels and palmitate oxidation rate correlate with ejection fraction in the infarcted rat heart. Cardiovasc Res 2006;72(3):430-437. doi:10.1016/j.cardiores.2006.08.020, PMID:17034771.
- 437. doi:10.1016/j.cardiores.2006.08.02, PMID:170347/1.
 [41] Dávila-Román VG, Vedala G, Herrero P, de las Fuentes L, Rogers JG, Kelly DP, et al. Altered myocardial fatty acid and glucose metabolism in idiopathic dilated cardiomyopathy. J Am Coll Cardiol 2002;40(2):271–277. doi:10.1016/s0735-1097(02)01967-8, PMID:12106931.
 [42] Bedi KC Jr, Snyder NW, Brandimarto J, Aziz M, Mesaros C, Worth AJ, et al. Evidence for Intramyocardial Disruption of Lipid Metabolism and Increased
- Myocardial Ketone Utilization in Advanced Human Heart Failure. Circulation 2016;133(8):706-716. doi:10.1161/CIRCULATIONAHA.115.017545,
- [43] Wai T, Langer T. Mitochondrial Dynamics and Metabolic Regulation. Trends Endocrinol Metab 2016;27(2):105–117. doi:10.1016/j.tem.2015.12.001, PMID:26754340.
- [44] Youle RJ, van der Bliek AM. Mitochondrial fission, fusion, and stress. Science 2012;337(6098):1062–1065. doi:10.1126/science.1219855, PMID:22936770. doi:10.1126/science.1219855,
- [45] Xie M, Yu Y, Kang R, Zhu S, Yang L, Zeng L, et al. PKM2-dependent glycolysis promotes NLRP3 and AIM2 inflammasome activation. Nat Commun 2016;7:13280. doi:10.1038/ncomms13280, PMID:27779186.
- [46] Palsson-McDermott EM, Curtis AM, Goel G, Lauterbach MA, Sheedy FJ, Gleeson LE, et al. Pyruvate kinase M2 regulates Hif-1a activity and IL- 1β induction and is a critical determinant of the warburg effect in LPS-activated macrophages. Cell Metab 2015;21(1):65–80. doi:10.1016/j.
- cmet.2014.12.005, PMID:25565206. [47] Chen X, Chen S, Yu D. Protein kinase function of pyruvate kinase M2 and cancer. Cancer Cell Int 2020;20(1):523. doi:10.1186/s12935-020-01612-1, PMID:33292198.
- [48] Esmaeili Z, Niaz Q, Saffari PM, Dehpour AR, Rezayat SM, Jazaeri F. Evaluation of the effect of heat shock protein 70 targeted drugs on cirrhotic cardiomyopathy in biliary cirrhotic rats. Life Sci 2021;273:119261. doi:10.1016/j.lfs.2021.119261, PMID:33652036.
 [49] Moheimani HR, Amiriani T, Alizadeh AM, Jand Y, Shakiba D, Ensan PS,
- et al. Preconditioning and anti-apoptotic effects of Metformin and Cyclosporine-A in an isolated bile duct-ligated rat heart. Eur J Pharmacol 2021;893:173807. doi:10.1016/j.ejphar.2020.173807, PMID:33359222.